DRUG DELIVERY
2022, VOL. 29, NO. 1, 1951–1958
https://doi.org/10.1080/10717544.2022.2089298

Taylor & Francis
Taylor & Francis Group

RESEARCH ARTICLE

OPEN ACCESS Check for updates

Targeted peptide-modified oxidized mesoporous carbon nanospheres for chemo-thermo combined therapy of ovarian cancer *in vitro*

Shanshan Wang[a], Wei Wu[a], Ying Liu[a], Chunhui Wang[a], Qing Xu[a], Qianzhou Lv[a], Rongqin Huang[b] and Xiaoyu Li[a]

[a]Department of Pharmacy, Zhongshan Hospital, Fudan University, Shanghai, China; [b]School of Pharmacy, Key Laboratory of Smart Drug Delivery, Ministry of Education, Fudan University, Shanghai, China

ABSTRACT

Ovarian cancer remains one of serious hazards to human health due to many drawbacks of existing available treatment options. In this study, a multifunctional chemo-thermo combined therapy nanoplatform (OMCNPID) was successfully prepared, which is composed of I_6P_8 peptide as a targeting moiety to interleukin-6 receptors (IL-6Rs), oxidized mesoporous carbon nanospheres (OMCN) as a near infrared (NIR)-triggered drug carrier and doxorubicin (DOX) as a chemotherapeutic drug and fluorescent agent. The synthesized multifunctional nanoplatform displayed high storage capacity for drugs and excellent photothermal properties. Besides, DOX was rapidly released from OMCNPID at the condition of low pH and NIR laser irradiation due to the dissociation of DOX from graphitic cores of OMCN. *In vitro* experimental results verified that OMCNPID could be markedly taken up by SKOV-3 monolayer cells and tumor spheroids, and revealed a remarkable synergistic chemo-photothermal effect against ovarian cancer. All the results demonstrated that OMCNPID is a pH/NIR dual-stimulus responsive nanoplatform and can achieve efficient chemo-thermo combined therapy.

ARTICLE HISTORY
Received 23 May 2022
Revised 2 June 2022
Accepted 6 June 2022

KEYWORDS
I_6P_8 peptide; OMCN; IL-6R; chemotherapy; PTT

1. Introduction

Ovarian cancer is a dominant cause of gynecologic malignancy-related death worldwide (Menon et al., 2021). Despite cytoreductive surgery and conventional chemotherapy, clinical data have indicated that the five-year survival rate with advanced stage is no more than 25% (Lheureux et al., 2019). This high mortality rate is attributed to lots of factors, including lack of effective treatment modalities, insufficient drug dosage to diseased regions, severe side effects, multidrug resistance and nonspecific drug delivery (Dai et al., 2020; Kim et al., 2021; Zhang et al., 2021). With this understanding, it is urgent to explore innovative therapeutic strategies to address these challenges for therapy of ovarian cancer.

Recently, multimodal therapy which simultaneously administers two or more monotherapies like chemotherapy, photothermal therapy (PTT), immunotherapy, gene therapy and photodynamic therapy, have offered a myriad of opportunities to achieve excellent outcomes (Gotwals et al., 2017; Wang et al., 2019; Zhan et al., 2020; Hao et al., 2021; Tang et al., 2021). Among the many cancer treatments, chemotherapy, which uses drugs such as DOX, platinum and paclitaxel to destroy or damage cancer cells, is remain the indispensable treatment for ovarian cancer (Harter et al., 2010; Chuan et al., 2021; Uruski et al., 2021). Hence, the burgeoning research interests have been focused on combining chemotherapy with other types of antitumor treatment including PTT. PTT, a well-established treatment mode, has recently emerged as an efficient minimally invasive therapy. PTT employs hyperthermia generated from the absorbed near-infrared (NIR) light by photothermal agents to ablate cancer cells and offers a series of distinct merits, including deep penetration, precise spatial-temporal selectivity, minimal trauma to health tissues and enhanced sensitivity of chemotherapy (Kim et al., 2016; Pallavicini et al., 2021). With advances in nanotechnology, the therapeutic efficacy can be further enhanced by employment of multifunctional nanomaterials as PTT agents, which will enable additional drug carrier or/and cancer imaging functionalities and make the increase of the drug accumulation at tumor sites possible. As such, PTT agents mainly focus on various noble-metal nanomaterials, 2 D-transition metal dichalcogenides, Cu-based semiconductor nanomaterials and carbon-based nanomaterials (Jain et al., 2008; Huang et al., 2017; Levin et al., 2019; Murugan et al., 2019; Wang et al., 2020). In our previous work, oxidized mesoporous carbon nanospheres (OMCN) could been regarded as prospective PTT reagents and nanocarriers due to their outstanding photothermal conversion ability and excellent drug loading capacity (Wang et al., 2017). Therefore, it is

CONTACT Rongqin Huang rqhuang@fudan.edu.cn School of Pharmacy, Key Laboratory of Smart Drug Delivery, Ministry of Education, Fudan University, Shanghai, China; Xiaoyu Li lixiaoyulxb@163.com Department of Pharmacy, Zhongshan Hospital, Fudan University, Shanghai, China.

reasonable to expect that the synergistic therapy of PTT and chemotherapy based on OMCN could enhance the effectiveness of ovarian cancer treatment. Besides, internal (acidic condition) and external (NIR) stimulation are beneficial to improve the drug release from carbon-based nanomaterials (including OMCN), which relies on the absorption of some aromatic drugs via simple π-stacking and the remarkable photothermal sensitivity (Yaghoubi & Ramazani, 2020; Do et al., 2021). However, no study was reported to investigate the employment of OMCN-based nanoplatform for treating ovarian cancer.

Besides, some nanoplatforms prone to accumulate inside tumor sites with a passive manner through the enhanced permeability and retention (EPR) effect. However, this passive manner has limitations due to its random delivery form. Active tumor targeting has been achieved by surface modification of nanoplatforms with ligands or antibodies, which may realize more accurate tumor delivery. A novel peptide I_6P_8 (sequenced CLSLITRL) was screened by a phage display technology on the cells expressing interleukin-6 receptor (IL-6R) (Wang et al., 2017). In this regard, for IL-6R overexpressed tumors, I_6P_8 may be a potential ligand for targeting delivery of drugs. Also, studies have revealed that IL-6R is significantly overexpressed in ovarian cancer cells, but is sub-expressed in normal tissues (Rath et al., 2010; Coward et al., 2011). Hence, I_6P_8 peptide was selected for designing nanoplatform to target ovarian cancer.

In this work, we designed a simple but versatile DOX-loaded OMCN nanoplatform to realize combined chemotherapy and PTT, by decorating the I_6P_8 peptide to target the IL-6R overexpressed in ovarian cancer cells. Our results demonstrated that the nanoplatform displayed high drug loading ability, excellent photothermal effect and pH- and thermo-triggered drug release. Furthermore, *in vitro* ovarian cell culture models were used to verify the tumor specificity, cellular uptake pathway and antitumor activity of the nanoplatform.

2. Materials and methods

2.1. Materials

SINOPHARM (Shanghai, China) provided the raw ingredients for the production of OMCNPID, including phenol, NaOH, formalin, N-Hydroxysuccinimide (NHS) and other reagents, while Sigma-Aldrich (St. Louis, USA) provided the triblock copolymer Pluronic F127 and the live-dead kit. JenKem Technology (Beijing, China) provided Maleimide PEG Amine (NH_2-PEG_{3500}-MAL) and Methoxy PEG Amine (NH_2-PEG_{3500}-OMe); ZiYu Biotech (Beijing, China) supplied the I_6P_8 peptide; Huafeng United Technology (Beijing, China) supplied the doxorubicin (DOX); and Dojindo Laboratories (Kumamoto, Japan) provided the Cell Counting Kit-8 (CCK-8) for this study.

2.2. Synthesis and surface modification of OMCN

In a typical synthesis (Wang et al., 2017), phenol (0.6 g) and formalin aqueous phase (37 wt percent, 2.1 mL) were mixed in a NaOH aqueous medium (0.1 M, 15 mL) and agitated for 0.5 hours at 70 °C. Then triblock copolymer Pluronic F127 aqueous solution (0.064 g/mL, 15 mL) and deionized water (50 mL) were then added, agitating for 2 hours and 18 hours respectively. The reaction solution was then diluted with distilled water (56 mL) and heated for 24 hours at 130 °C. Ultra-centrifugation was used to collect the product, which was then cleaned with deionized water before being freeze-dried. Finally, for carbonization, the freeze-dried powder was put in a nitrogen flow and heated up programmatically. To obtain OMCN, the aforementioned synthesized carbon powder was refluxed at 60 °C for 4 hours in a mixed acid solution (VH_2SO_4/$VHNO_3$ =3/1).

Two-step processes were used to modify the surface of OMCN. To activate the carboxylic group, OMCN (4 mg) was submerged in an EDC/NHS/MES solution (40 mg EDC and 72 mg NHS in 4 mL MES buffer, pH 6.0) and swirled at room temperature for 2 hours. Then, ultra-centrifugation at 4500 g for 5 minutes was used to purify the product. Excessive NH_2-PEG_{3500}-MAL (5.6 mg) and NH_2-PEG_{3500}-OMe (5.6 mg) were then added to the MES buffer solution (pH 6.0, 8 mL) and mixed for 4 hours, harvesting PEGylation OMCN (OMCNP). The I_6P_8 peptide (2 mg) was then added to OMCNP suspension (PBS buffer, pH 7.0) and stirred for 24 hours at ambient temperature, obtaining I_6P_8 peptide-modified OMCNP (OMCNPI). Finally, ultra-centrifugation was used to eliminate any remaining compounds.

2.3. DOX loading

DOX was loaded prior to the above-mentioned OMCN surface modification for maximal drug loading. In short, the prepared OMCN and DOX with equal mass were submerged in PBS buffer (pH 7.0) and swirled in the dark for 24 hours. Ultra-centrifugation was used to collect the product, and the unloaded DOX remained in the supernatant. Subtracting the supernatant DOX from the total DOX measured using a fluorescence spectrophotometer yielded the mass of DOX loaded in OMCN. The following mathematical formulae were used to determine OMCNPID's drug loading capacity (DLC, %) and encapsulation efficiency (EE, %):

$$\mathrm{DLC}(\%)=\frac{\text{mass of DOX loaded in OMCN}}{\text{mass of nanocarrier}}\times 100\%$$

$$\mathrm{EE}(\%)=\frac{\text{mass of DOX loaded in OMCN}}{\text{mass of total DOX}}\times 100\%$$

2.4. Characterizations

A dynamic light scattering (DLS) spectrometer and a transmission electron microscope (TEM) were used to measure particle size, zeta potential and morphology, respectively. A Fourier transform infrared (FT-IR) spectrometer was used to measure the FT-IR spectra. And a UV-vis spectrophotometry was used to measure the absorption spectra. A fluorescence spectrophotometer was used to record the fluorescence

spectra. A laser scanning confocal microscope or an inverted fluorescence microscope was used to obtain all cell pictures.

2.5. Photothermal effect

Various concentrations of OMCNPI aqueous solution (0, 15, 30, 45, 60, and 75 μg/mL) were placed in plastic tubes and irradiated with an 808-nm laser at a series of power densities (2, 3, and 4 W/c m^2) for 5 minutes to determine the photothermal effect of OMCNPI. An infrared thermal camera was used to continually monitor the temperature of OMCNPI aqueous solution.

2.6. In vitro drug release profiles

Equal volumes of OMCNPID solutions (2 mg/ml) were put in dialysis tubing and then submerged in 10 mL three different PBS with pH of 5.0, 6.0, and 7.4 in the dark with moderate shaking at 37 °C to investigate DOX releasing amount. At the specified intervals, aliquots (1 mL) were withdrawn and replaced with an equivalent volume of fresh PBS. A similar method was followed for the NIR-triggered groups, but the solution was irradiated with an NIR laser (3 W/cm^2) for 5 minutes before the release solution was withdrawn. A microplate reader was used to track the amount of DOX release.

2.7. Cell culture

The Cell Bank of the CAS provided two distinct cell lines for this study: human ovarian cancer epithelial cells (SKOV-3 cells) and normal human ovarian epithelial cells (IOSE-80 cells). SKOV-3 cells were typically cultured in McCOY's 5 A medium, which included 10% heat-inactivated fetal bovine serum (FBS), 2.2 g/L $NaHCO_3$, 1% L-glutamine and penicillin-streptomycin. IOSE-80 cells were cultured in RPMI 1640 medium supplemented by 10% FBS, 1% L-glutamine and penicillin-streptomycin. In a 5% CO_2 water-saturated incubator, cells were kept at 37 °C.

2.8. Western blot analysis

In 6-well plates, SKOV-3 and IOSE-80 cells were cultured at a density of 1×10^5 cells per well, respectively. The cells in each well were collected and lysed with cell lysis buffer after 24 hours of culturing. Cell lysates were centrifuged at 13500 rpm for 10 minutes at 4 °C and then the supernatant was collected and total protein content was determined using a BCA Protein Assay Kit. Following that, 30 μg proteins were added to 10% SDS-PAGE gels and then transferred to PVDF membranes. The membrane was treated overnight with a primary rabbit anti-IL-6R antibody (1:1000 dilution) or mouse anti-GAPDH antibody (1:1000 dilution) and further cultured with HRP-conjugated secondary goat anti-rabbit antibody (1:1000 dilution) or goat anti-mouse antibody (1:1000 dilution) for 1 hour. A chemiluminescence technique was used to measure the amounts of IL-6R expression in SKOV-3 and IOSE-80 cells.

2.9. Cellular uptake

SKOV-3 and IOSE-80 cells were cultured at 1×10^5 cells/dish in confocal cell culture dish to test targeting cellular uptake. 1.5 mL media containing OMCNPID and OMCNPD with a DOX content of 50 μg/mL was individually introduced to the cells after 24 hours of adhesion and cultured for 1 hour at 37 °C. SKOV-3 cells were treated with excess I_6P_8 peptide for 20 minutes at 37 °C before aforesaid 1 hour incubation with OMCNPID to examine I_6P_8 peptide-mediated cellular uptake by ovarian cancer cells. SKOV-3 cells were treated with 50 μg/mL OMCNPID for 1 hour at 37 °C and 4 °C respectively to investigate energy-dependent cellular uptake. The cells were seen using a laser scanning confocal microscope after being rinsed and immobilized.

2.10. Tumor spheroid penetration

SKOV-3 cells were cultured in 48-well plates covered with 2% sterile low-melting-point agarose to create three-dimensional (3 D) tumor spheroids. Tumor spheroids were treated for 12 hours with OMCNPID and OMCNPD, respectively, seven days later. After being rinsed with cold PBS and fixed with 4% paraformaldehyde, a laser scanning confocal microscope was used to scan the tumor microspheres every 20 μm from top to bottom.

2.11. In vitro antitumor activity

A live-dead kit was used to test the cytotoxicity of the drug-loaded nanoplatform in SKOV-3 cells. Briefly, SKOV-3 cells were cultured at a density of 1×10^4 cells/well in 96-well plates and incubated for 24 hours. Then cells were treated with saline, OMCNPI, OMCNPI + NIR, OMCNPID and OMCNPID + NIR with OMCN concentration at 45 μg/mL. After a 6-hour incubation period, the photothermal treatment groups' cells were subjected to a 3 W/cm^2 NIR laser at 808 nm for 5 minutes. All the cells were then rinsed and cultured for another 42 hours in new complete medium. After the incubation period, a live-dead kit was used to assess cytotoxicity, and a CCK-8 kit was used for quantitative evaluation.

2.12. Statistical analysis

The mean ± standard deviation was displayed for each value (SD). Analysis of variance (ANOVA) was used to conduct statistical analysis of multigroup trials, with a P value < 0.05 regarded statistically significant.

3. Results and discussion

3.1. Synthesis and characterizations

As shown in Scheme 1, the fabrication procedure of OMCNPID included two main steps. The first step was DOX loading into the mesopores of OMCN, and the second step was I_6P_8 peptide fuzing on the surface of OMCN via the PEG modification. By calculating with fluorescence, the DLC (%) and EE (%) of

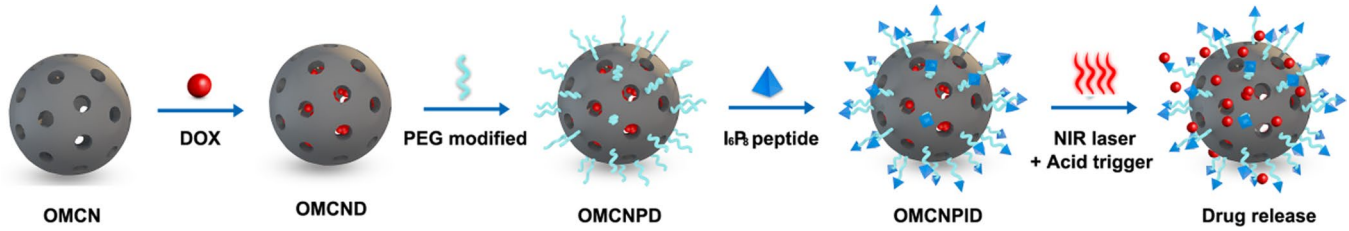

Scheme 1. Schematic illustration of synthetic process of OMCNPID and its drug release.

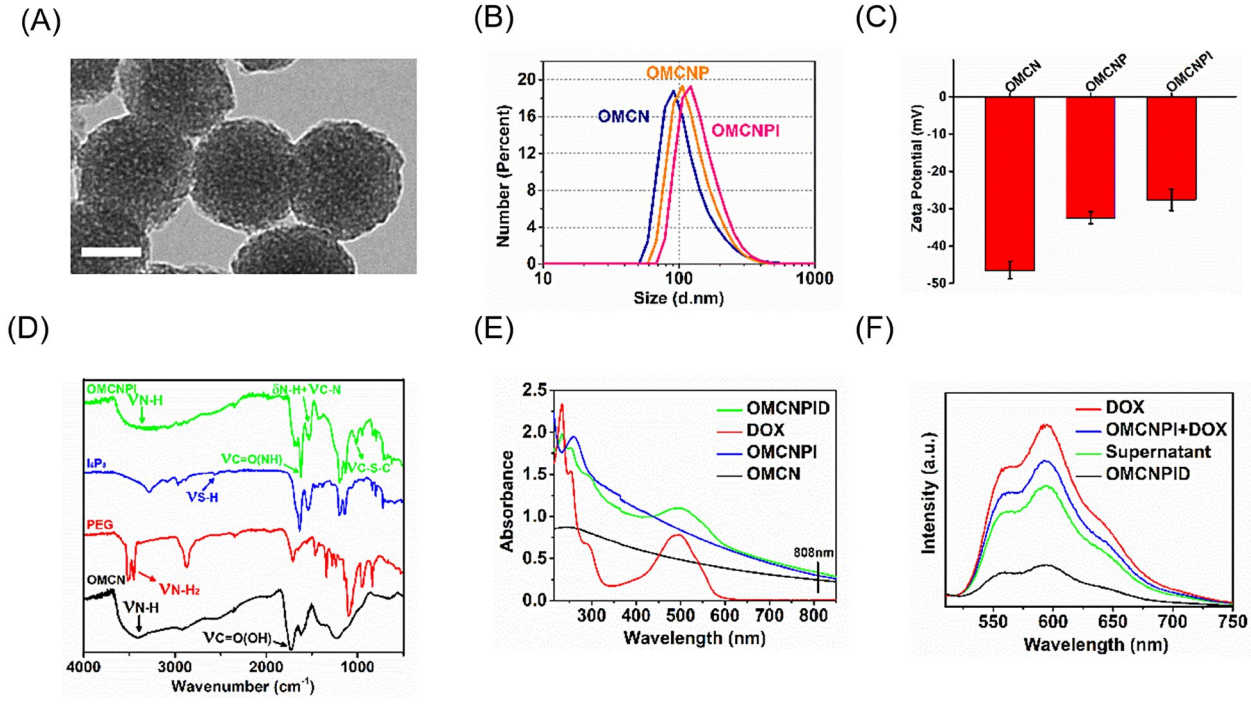

Figure 1. Characterizations of nanoparticles. (A) TEM image of OMCN. Bar = 50 nm. (B) DLS and (C) zeta potential measurements of OMCN, OMCNP and OMCNPI. Data were presented as mean ± S.D. ($n = 3$). (D) FT-IR spectra of OMCN, PEG, I_6P_8 and OMCNPI. (E) UV-vis-NIR spectra of OMCN, OMCNPI, DOX and OMCNPID. (F) Fluorescence spectra of free DOX, the mixture of OMCNPI and DOX, supernatant and OMCNPID.

OMCNPID reached up to approximately 86.4%, which were much higher than those of other carriers (Xu et al., 2020; Dinçer et al., 2022; Galhano et al., 2022).

To confirm the synthesis, TEM, particle size, zeta potential, FT-IR, UV-vis-NIR and fluorescence spectra were carried out. The morphology of OMCN was characterized by TEM. Figure 1A revealed OMCN had a regular near-spherical shape with mesoporous structure and were well-dispersed in water. Surface decoration with PEG and I_6P_8 peptides increased the average hydrodynamic size determined by dynamic laser scattering (DLS) from 131.6 nm for OMCN to 164.1 nm for OMCNP and 198.3 nm for OMCNPI (Figure 1B). Successful modification was further proved by the surface zeta potential in water. The zeta potential of OMCN was highly negative (-46.5 ± 2.3 mV) attributable to the fact that there are a number of carboxy groups on their surface (Figure 1C). On account of the PEGylation shielding effect and the covalent binding of positive-charged I_6P_8 peptide, the zeta potentials demonstrated a growing tendency (-32.4 ± 1.6 mV for OMCNP and −27.6 ± 2.9 mV for OMCNPI).

Moreover, the successful coupling of PEG and conjugation of I_6P_8 peptide on OMCN were evaluated by FT-IR analysis. In the FT-IR spectrum of OMCN, the broad absorbance appeared in around 3400 cm^{-1} was ascribed to the secondary amine stretching vibration, while the peaks at 1735 cm^{-1} was designated to carbonyl stretching vibration of the carboxy groups (Figure 1D). After OMCN reacted with PEG and I_6P_8, the significant bands at 3445 cm^{-1} and 3516 cm^{-1} (primary amide stretching vibration, $\nu N\text{-}H_2$) which belong to PEG and 2550 cm^{-1} (S-H stretching vibration, νS-H) which belongs to I_6P_8 were disappeared. Meanwhile, some new characteristic peaks appeared at 1620 cm^{-1} (amide carbonyl stretching vibration, νC = O(NH)), 1540 cm^{-1} (amide II band, δN-H + νC-N) and 1013 cm^{-1} (C-S-C stretching vibration, νC-S-C) indicated the successful synthesis of the OMCNPI. As can been seen in Figure 1E, the UV − vis absorption curve of OMCNPID exhibited a relatively strong peak at 488 nm, which belongs to the characteristic absorption of DOX, suggesting that DOX was successfully loaded into OMCNPI. In addition, obvious absorption in the NIR region (including 808 nm) was exhibited in the UV − vis spectra of OMCN, OMCNPI and OMCNPID, indicating that OMCN-based carriers were suitable candidates for PTT upon 808 nm laser irradiation. Figure 1F demonstrated the fluorescence spectra of various products in the process of

fabricating OMCNPID (Ex = 488 nm). It can be noted that the fluorescence intensity of OMCNPID was much inferior to that of free DOX and the mixture of OMCNPI and DOX at equal concentrations, which might be owing to the fact that the fluorescence signal of DOX would be quenched by OMCN when they aggregated at high concentrations.

3.2. Photothermal effect

The *in vitro* photothermal performance of OMCNPI was evaluated by detecting the temperature change of OMCNPI aqueous solutions at different concentrations during 5 minutes laser irradiation. The temperature profiles and photothermal images were showed in Figure 2. As expected, the NIR-triggered photothermal effect was highly dependent on the concentration of OMCNPI and laser power intensity. For pure water (0 μg/mL OMCNPI), the temperature increased minimally after irradiation for 5 minutes. On the contrary, the temperature of OMCNPI aqueous solutions increased rapidly when the concentration increased from 15 to 75 μg/mL at the same power intensity (Figure 2A). In the meantime, the temperature of OMCNPI aqueous solutions gradually increased as the power intensity ranging from 2 W/cm^2 to 4 W/cm^2 (Figure 2B). Moreover, the temperature of 45 μg/mL OMCNPI aqueous solution could exceed 50 °C under a power density of 3 W/cm^2, reaching the biological photolethal limit of the cells. These findings revealed that OMCNPI could serve as a great potential near-infrared agent for PTT.

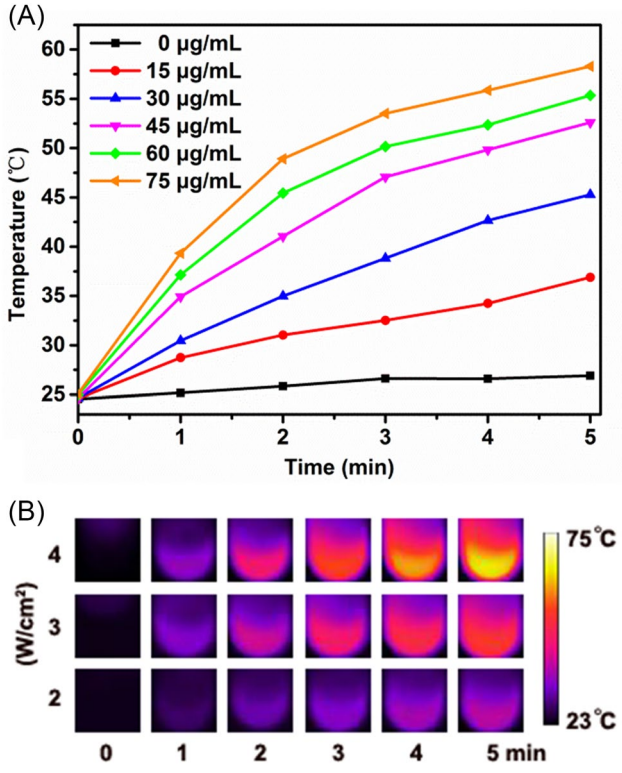

Figure 2. Photothermal effect of OMCNPI. (A) Temperature profiles of OMCNPI aqueous solution with different concentrations (0, 15, 30, 45, 60 and 75 μg/mL) by the 808-nm laser with a power density of 3.0 W/cm^2 for 5 minutes. (B) Photothermal images of OMCNPI aqueous solution (45 μg/mL) recorded after an 808-nm laser irradiation with a power density ranging from 2 W/cm^2 to 4 W/cm^2 for 5 minutes.

3.3. In vitro drug release profiles

As illustrated in Figure 3, the release of drug from OMCNPID triggered by pH change and NIR laser irradiation were investigated. It was observed that only about 19.5% DOX was released from OMCNPID in pH 7.4 PBS after 48 hours, which validated the stable loading of DOX into OMCNPID under physiological condition (Figure 3A). However, the cumulative drug release in pH 6.0 PBS and pH 5.0 PBS increased up to 47.2% and 66.9% within the same time period, suggesting that the DOX release from OMCNPID was significantly pH-triggered. This phenomenon could be ascribed to the protonation of amino groups on DOX under acidic conditions, thus increasing electrostatic repulsion between DOX and graphitic cores of OMCN. Additionally, the amount of DOX released from OMCNPID after exposure to NIR laser for 5 minutes at predetermined time demonstrated a noticeable increase in comparison with that without NIR laser exposure in all release conditions (Figure 3B). The cumulative release amount was 82.4% under the condition of pH 5.0 PBS and NIR laser irradiation, which was more than that under the single condition of pH 5.0 PBS (66.9%), implying that OMCNPID had NIR-triggered drug release properties. Consequently, OMCNPID

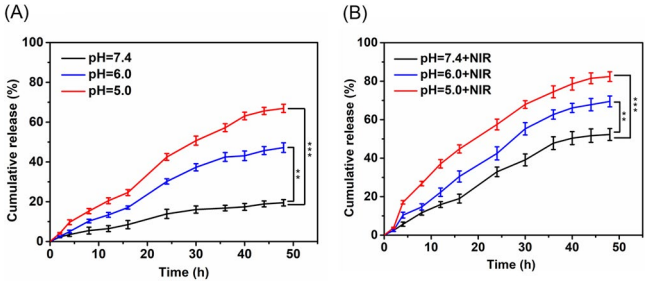

Figure 3. Drug release profiles of OMCNPID. Drug release profiles of DOX from OMCNPID under different pH conditions (pH 5.0, 6.0 and 7.4) without (A) or with (B) the NIR laser irradiation at 3 W/cm^2. Data were presented as mean ± S.D. ($n = 3$). $^{**}p < 0.01$, $^{***}p < 0.001$.

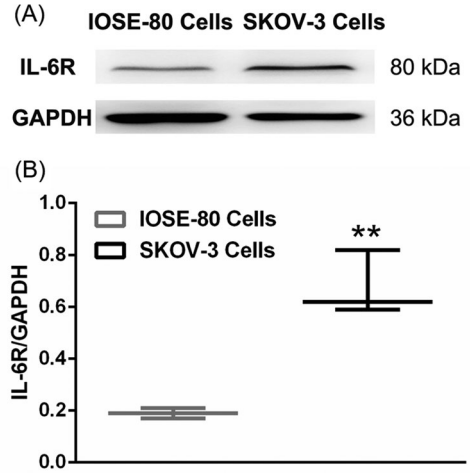

Figure 4. The results of western blot assay. (A) Protein expression level of IL-6R in IOSE-80 cells and SKOV-3 cells. (B) Densitometric analysis of IL-6R levels normalized to GAPDH levels ($n = 3$). $^{**}p < 0.01$.

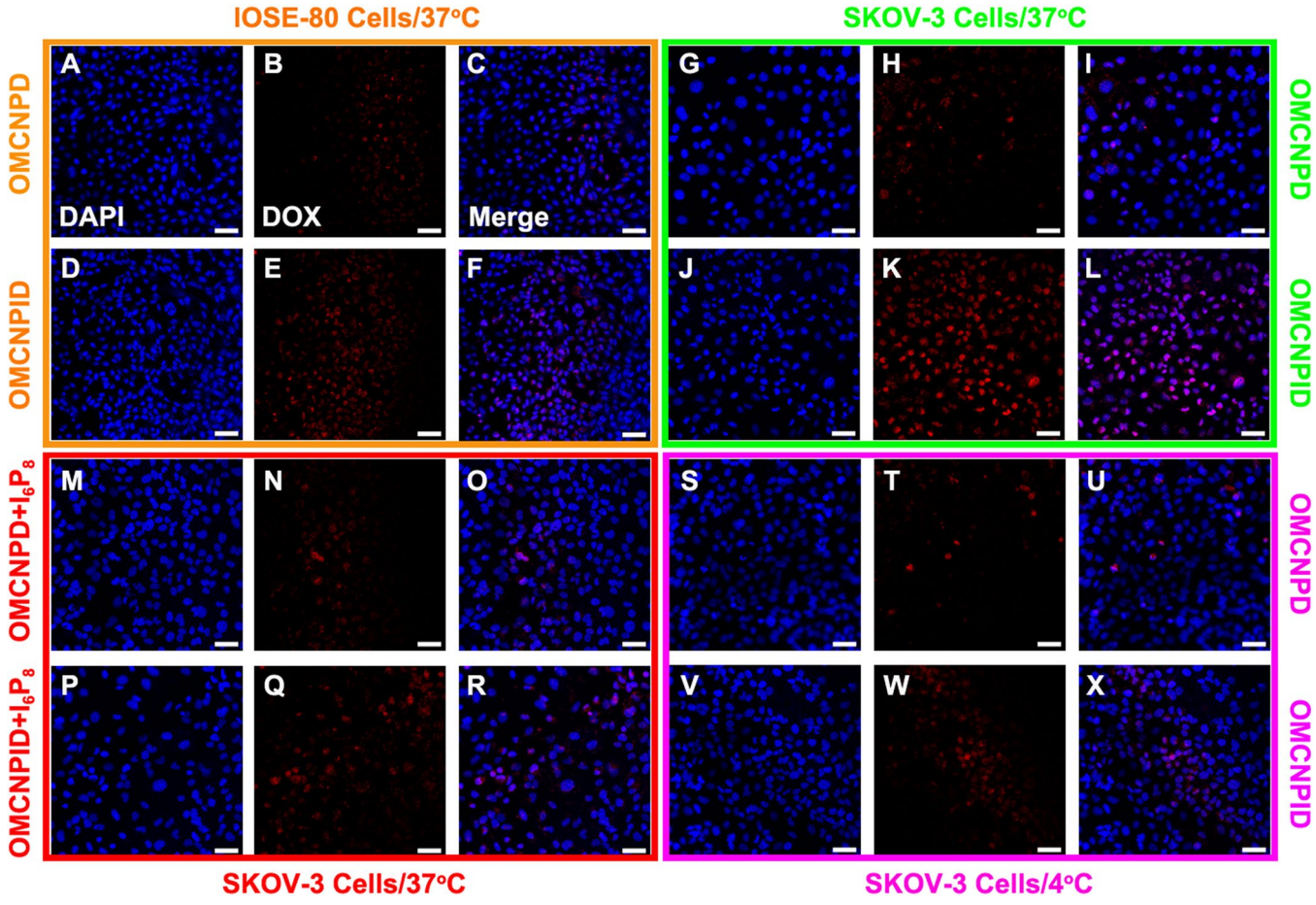

Figure 5. Cellular uptake of OMCNPD and OMCNPID. (A-L) Fluorescent images of IOSE-80 and SKOV-3 cells incubated with OMCNPD or OMCNPID, respectively. (M-R) Fluorescent images of SKOV-3 cells incubated with OMCNPD or OMCNPID with excess free I_6P_8 peptide. (S-X) Fluorescent images of SKOV-3 cells incubated with OMCNPD or OMCNPID at 4 °C. Bar = 100 μm.

could realize remotely controlled drug release under the dual-stimulus including tumor microenvironment (acidic condition) and outer environment (NIR) to decrease the side effect and enhance the synergistic therapeutic effect.

3.4. IL-6R expression level in specific cells

IL-6R expression level was testified on both SKOV-3 cells and IOSE-80 cells by western blot (Figure 4). Densitometry studies revealed the high IL-6R expression on SKOV-3 cells, which was consistent with previous reports (Coward et al., 2011), making SKOV-3 cells an ideal model for ovarian cancer targeting delivery and treatment. Nevertheless, there was low IL-6R expression on IOSE-80 cells, which might be deemed as a negative control to assess the function of the targeted IL-6R. Thus, this study utilized SKOV-3 cells and IOSE-80 cells for the evaluation of targeting efficiency of OMCNPID.

3.5. Cellular uptake

The tumor-targeting capability of different formulations was assessed by the uptake in SKOV-3 cells and IOSE-80 cells. As displayed in Figure 5A–L, higher fluorescence intensity of OMCNPID was found in SKOV-3 cells as compared with that of OMCNPD. Also, the fluorescence intensity of OMCNPID in SKOV-3 cells was far superior to that in IOSE-80 cells, suggesting that I_6P_8 on nanoplatform surface could significantly facilitate the nanoplatform targeting to SKOV-3 cells. However, there was no striking difference in the fluorescence intensity between the OMCNPID and OMCNPD in IOSE-80 cells, indicating the existence of I_6P_8 did not influence the uptake behavior of the nanoplatform by IOSE-80 cells. This was most likely due to the apparently higher expression on IL-6R in SKOV-3 cells than that on IOSE-80 cells. In the competitive inhibition assay, cells treated by OMCNPID with excess free I_6P_8 peptide to saturate IL-6R showed lower fluorescence intensity as compared to those treated by OMCNPID without free I_6P_8 peptide (Figure 5M–R). This result demonstrated a receptor-mediated process and I_6P_8 has high transcytosis ability mediated by IL-6R for cellular uptake into SKOV-3 cells. In addition, the energy-dependent endocytosis was observed. As visualized in Figure 5S–X, the cellular uptake of OMCNPID in SKOV-3 cells was remarkably inhibited in 4 °C compared with 37 °C. The temperature-dependent characteristic displayed the involvement of energy-dependent processes during the IL-6R-mediated endocytosis.

3.6. Permeation into 3D tumor spheroids

The above findings confirmed the potential of OMCNPID as an efficient formulation with excellent cellular internalization

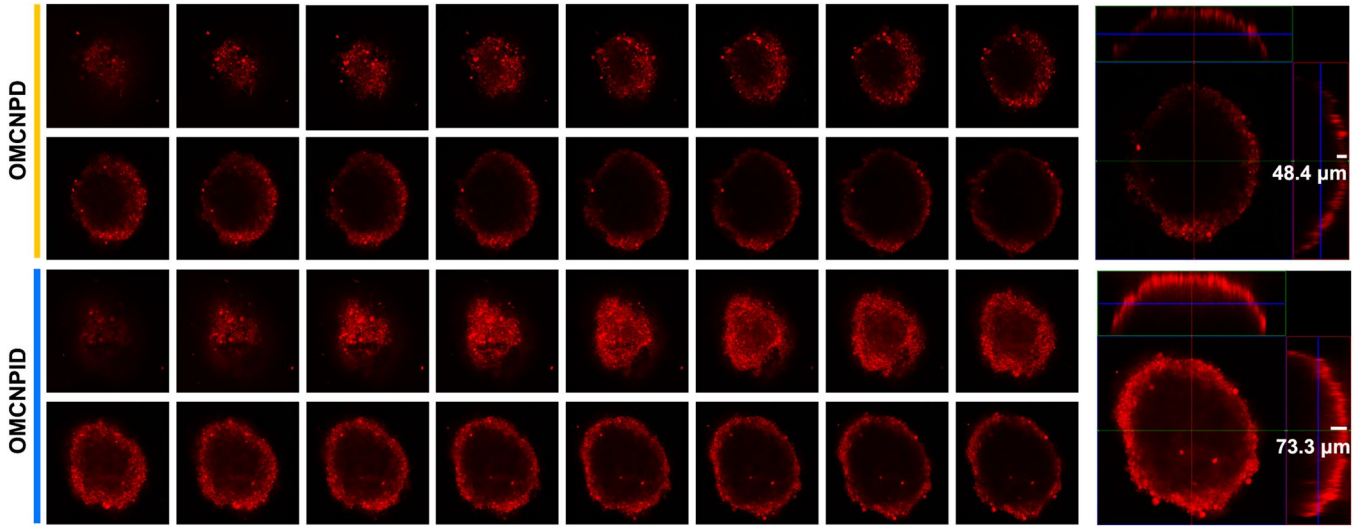

Figure 6. Representative fluorescent images and orthogonal images of SKOV-3 tumor spheroids at the determined scanning layers after incubation with OMCNPD and OMCNPID for 12 h.

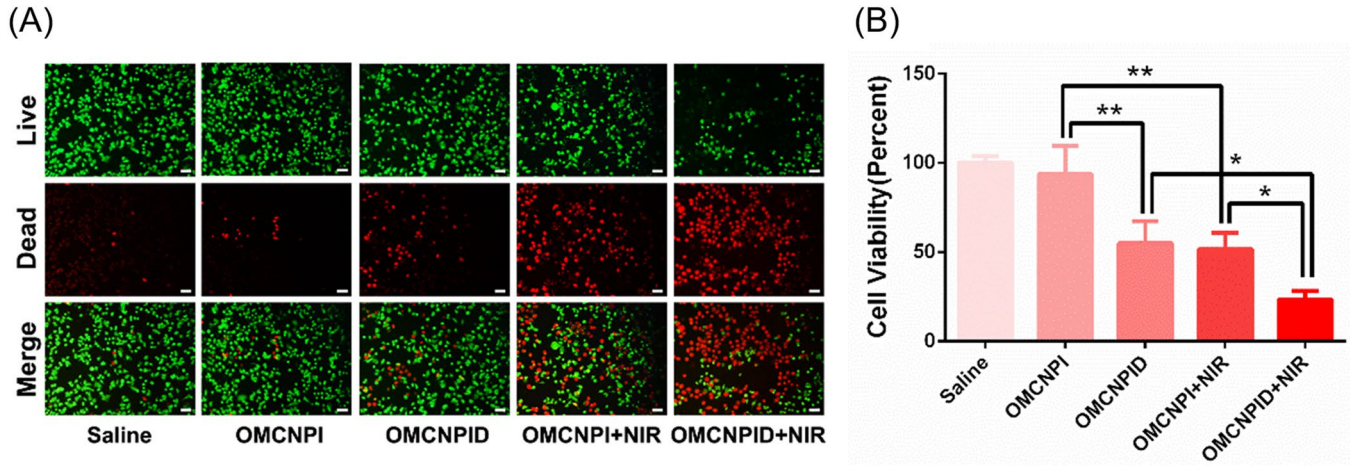

Figure 7. *In vitro* antitumor activity. Live-dead assay (A) and CCK-8 assay (B) on SKOV-3 cells after incubated with saline, OMCNPI, OMCNPI + NIR, OMCNPID and OMCNPID + NIR. Bar = 100 μm. Data were presented as mean ± S.D. ($n = 3$). *$p < 0.05$, **$p < 0.01$.

in a 2 D SKOV-3 cell cultured monolayer model. However, the cellular uptake by monolayer cells may not reflect the tumor-accumulating effect of different formulations accurately because the drugs must be transported into the cells in the core regions of tumor, not just the surface cells. Considering this, 3D tumor spheroid could serve as a reliable *in vitro* evaluation model for investigating penetration behavior of different formulations. The penetrating ability of different formulations was monitored by confocal microscopy after 12 h incubation with SKOV-3 tumor spheroids. For qualitative analysis, the fluorescence intensity observed in SKOV-3 tumor spheroids treated with OMCNPID was much more prominent than that of OMCNPD (Figure 6). For quantitative analysis, OMCNPID penetrated around 73.3 μm into SKOV-3 tumor spheroids, whereas OMCNPD showed an average penetration depth of only 48.4 μm. These results suggested that I_6P_8 decoration could effectively improve nanoplatform penetration into SKOV-3 tumor spheroids. The excellent permeation ability was indispensable to ovarian cancer treatment.

3.7. In vitro antitumor activity

The *in vitro* antitumor activity of different formulations was assessed via live-dead assay by staining the tumor cells with Calcein-AM and PI. In this assay, live cells stained by Calcein-AM glowed green fluorescence, whereas dead cells stained by PI exhibited red fluorescence. As visualized in Figure 7A, cells treated with saline or OMCNPI exhibited the darkest red fluorescence indicating that there were no significant dead cells. This suggested that the drug nanocarrier, OMCNPI, could cause negligible cytotoxicity. Notably, chemo-thermo combined therapy (OMCNPID + NIR group) displayed higher cell death compared to that in monotherapy (OMCNPID group or OMCNPI + NIR group). Then the antitumor activity was further quantitative validated by CCK-8 assay. As seen in Figure 7B, chemo-thermo combined therapy group resulted in lowest SKOV-3 cell viability and the cytotoxicity was about 1.69- and 1.58-fold of that of OMCNPID group and OMCNPI + NIR group, respectively. Overall, the results clearly revealed that the chemo-thermo

combined therapy exhibited significantly enhanced antitumor efficacy *in vitro,* which was probably due to the targeting I_6P_8 peptide for better cellular uptake and synergistic effect of different therapies. Certainly, further *in vivo* experiment is necessary to evaluate the antitumor efficacy before a final statement.

4. Conclusion

This study demonstrated that OMCNPID was fabricated as a multifunctional anti-cancer nanoplatform for chemo-thermo combined therapy of ovarian tumors. Based on the *in vitro* observations, the as-prepared OMCNPID revealed suitable size, high storage capacity for drugs, satisfying photothermal ability and pH- and NIR-triggered DOX release effect. Here, DOX loaded in the nanoplatform and OMCNPI were utilized for chemotherapy and PTT, respectively. Cellular uptake and tumor spheroid penetration results respectively indicated that the conjugation of I_6P_8 peptide to OMCN significantly enhanced the IL-6R-mediated accumulation and penetration of DOX in both SKOV-3 monolayer cell and tumor spheroids. More importantly, OMCNPID showed remarkable antitumor efficacy *in vitro*, owing to the surface conjugation of targeting I_6P_8 peptide and excellent synergistic therapeutic effects. Therefore, the investigation validated that the multifunctional nanoplatform would open a potential new avenue for ovarian tumor therapy.

Disclosure statement

No potential conflict of interest was reported by the authors.

Funding

This work was supported by the grants from National Natural Science Foundation of China (82003278), Shanghai Sailing Program (18YF1403900) and Shanghai Key Clinical Specialist Construction Projects (shslczdzk06504).

References

Dinçer C, Getiren B, Gökalp C, et al. (2022). An anticancer drug loading and release study to ternary GO-Fe3O4-PPy and Fe3O4 @PPy-NGQDs nanocomposites for photothermal chemotherapy. Colloids Surf A 633:127791.

Chuan D, Mu M, Hou H, et al. (2021). Folic acid-functionalized tea polyphenol as a tumor-targeting nano-drug delivery system. Mater Des 206:109805.

Coward J, Kulbe H, Chakravarty P, et al. (2011). Interleukin-6 as a therapeutic target in human ovarian cancer. Clin Cancer Res 17:6083–96.

Dai J, Cheng Y, Wu J, et al. (2020). Modular peptide probe for pre/intra/postoperative therapeutic to reduce recurrence in ovarian cancer. ACS Nano 14:14698–714.

Do TTA, Grijalvo S, Imae T, et al. (2021). A nanocellulose-based platform towards targeted chemo-photodynamic/photothermal cancer therapy. Carbohydr Polym 270:118366.

Galhano J, Marcelo GA, Duarte MP, Oliveira E. (2022). Ofloxacin@Doxorubicin-Epirubicin functionalized MCM-41 mesoporous silica-based nanocarriers as synergistic drug delivery tools for cancer related bacterial infections. Bioorg Chem 118:105470.

Gotwals P, Cameron S, Cipolletta D, et al. (2017). Prospects for combining targeted and conventional cancer therapy with immunotherapy. Nat Rev Cancer 17:286–301.

Hao K, Lin L, Sun P, et al. (2021). Cationic flexible organic framework for combination of photodynamic therapy and genetic immunotherapy against tumors. Small 17:e2008125.

Harter P, Hilpert F, Mahner S, et al. (2010). Systemic therapy in recurrent ovarian cancer: current treatment options and new drugs. Expert Rev Anticancer Ther 10:81–8.

Huang X, Zhang W, Guan G, et al. (2017). Design and functionalization of the NIR-responsive photothermal semiconductor nanomaterials for cancer theranostics. Acc Chem Res 50:2529–38.

Jain PK, Huang XH, El-Sayed IH, El-Sayed MA. (2008). Noble metals on the nanoscale: optical and photothermal properties and some applications in imaging, sensing, biology, and medicine. Acc Chem Res 41:1578–86.

Kim J, Kim J, Jeong C, Kim WJ. (2016). Synergistic nanomedicine by combined gene and photothermal therapy. Adv Drug Deliv Rev 98:99–112.

Kim J, Shim MK, Cho YJ, et al. (2021). The safe and effective intraperitoneal chemotherapy with cathepsin B-specific doxorubicin prodrug nanoparticles in ovarian cancer with peritoneal carcinomatosis. Biomaterials 279:121189.

Levin T, Sade H, Binyamini RB, et al. (2019). Tungsten disulfide-based nanocomposites for photothermal therapy. Beilstein J Nanotechnol 10:811–22.

Lheureux S, Braunstein M, Oza AM. (2019). Epithelial ovarian cancer: evolution of management in the era of precision medicine. CA Cancer J Clin 69:280–304.

Menon U, Gentry-Maharaj A, Burnell M, et al. (2021). Ovarian cancer population screening and mortality after long-term follow-up in the UK Collaborative Trial of Ovarian Cancer Screening (UKCTOCS): a randomised controlled trial. The Lancet 397:2182–93.

Murugan C, Sharma V, Murugan RK, et al. (2019). Two-dimensional cancer theranostic nanomaterials: Synthesis, surface functionalization and applications in photothermal therapy. J Control Release 299:1–20.

Pallavicini P, Chirico G, Taglietti A. (2021). Harvesting light to produce heat: photothermal nanoparticles for technological applications and biomedical devices. Chemistry 27:15361–74.

Rath KS, Funk HM, Bowling MC, et al. (2010). Expression of soluble interleukin-6 receptor in malignant ovarian tissue. Am J Obstet Gynecol 203:230 e231–238.

Tang W, Han L, Duan S, et al. (2021). An aptamer-modified DNA tetrahedron-based nanogel for combined chemo/gene therapy of multidrug-resistant tumors. ACS Appl Bio Mater 4:7701–7.

Uruski P, Sepetowska A, Konieczna C, et al. (2021). Primary high-grade serous ovarian cancer cells are sensitive to senescence induced by carboplatin and paclitaxel in vitro. Cell Mol Biol Lett 26:44.

Wang X, Dai J, Wang X, et al. (2019). MnO2-DNAzyme-photosensitizer nanocomposite with AIE characteristic for cell imaging and photodynamic-gene therapy. Talanta 202:591–9.

Wang S, Li C, Meng Y, et al. (2017). MemHsp70 receptor-mediated multifunctional ordered mesoporous carbon nanospheres for photoacoustic imaging-guided synergistic targeting trimodal therapy. ACS Biomater Sci Eng 3:1702–9.

Wang S, Li C, Qian M, et al. (2017). Augmented glioma-targeted theranostics using multifunctional polymer-coated carbon nanodots. Biomaterials 141:29–39.

Wang H, Pan X, Wang X, et al. (2020). Degradable carbon-silica nanocomposite with immunoadjuvant property for dual-modality photothermal/photodynamic therapy. ACS Nano 14:2847–59.

Xu J, Shamul JG, Wang H, et al. (2020). Targeted heating of mitochondria greatly augments nanoparticle-mediated cancer chemotherapy. Adv Healthcare Mater 9:e2000181.

Yaghoubi A, Ramazani A. (2020). Anticancer DOX delivery system based on CNTs: Functionalization, targeting and novel technologies. J Control Release 327:198–224.

Zhan X, Nie X, Gao F, et al. (2020). An NIR-activated polymeric nanoplatform with ROS- and temperature-sensitivity for combined photothermal therapy and chemotherapy of pancreatic cancer. Biomater Sci 8:5931–40.

Zhang Y, Dong Y, Fu H, et al. (2021). Multifunctional tumor-targeted PLGA nanoparticles delivering Pt(IV)/siBIRC5 for US/MRI imaging and overcoming ovarian cancer resistance. Biomaterials 269:120478.